mixing (Figs. 3.10, 3.11). This process may explain the cessation of the Awoshiwo event that started on 24 September. There was a southerly wind on 26 September that brought oxygen-rich surface water into the northern shore area; the entire water column was replaced with this oxygen-rich water, which ended the Awoshiwo.

As discussed above, the southerly wind plays a significant role in supplying oxygen to deeper layers in the northern shore area; vertical mixing is accelerated and is discernible in an increase in the vertical eddy-diffusivity coefficient throughout the water column (Fig. 3.20). In the present case, the depth of the location at which the variation in vertical eddy-diffusivity coefficient was plotted was 4.1 m. It is implied from Fig. 3.20 that the entire water column at this location was well mixed on 28 September. However, a conspicuous increase in the vertical eddy-diffusivity coefficient, caused by a strong southerly wind (28 September) was detected only within layers shallower than 10 m in deeper locations. This means that the dissolved oxygen level can be enhanced by southerly winds in areas shallower than 10 m even in a stratified period. It also indicates that areas deeper than 10 m will experience anoxic conditions for longer periods. All locations at which bottom oxygen was depleted (i.e. less than 1.0 $mg.l^{-1}$) were deeper than 10 m (Figure 3.16 (a)). The bottom salinity profile on 28 September shows that the area that experienced a decrease in salinity due to vertical mixing was limited to the shallow northern coastal zone (Fig. 3.22). Even within the northern shore area, the bottom salinity over channels for navigation to the ports of Chiba and Funabashi and dredged areas was still high in spite of the southerly wind. The areas in which bottom salinity was higher than 32‰ corresponded to areas deeper than 10 m. The possibility of occurrence of anoxic bottom water was high within those areas.

We have discussed how the water flow in Tokyo Bay is influenced significantly by the wind. In particular, winds in a north-south direction have a strong impact on the water quality in the northern shore area. Three-dimensional views of contours of 30‰ isohalines and the surface area where salinity was higher than 30‰ are shown in Figure 3.23. These 4 plots represent the shape of upwelling and vertical mixing in the northern shore area induced by northerly winds. The surface area where salinity was higher than 30‰ was identical to the area that experiences Awoshiwo events frequently. These views show that our model can be applied successfully to the analysis of physical processes leading to Awoshiwo events.

3.5 References

Blumberg, A. F. and Goodrich, D. M. 1990. Modeling of wind-induced destratification in Chesapeake Bay.

Blumberg, A. F. and G. L. Mellor. 1987. A description of a three-dimensional coastal ocean circulation model, p. 1-16. In N. Heaps (ed.), Three-Dimensional Coastal Ocean Models. American Geophysical Union.

Blumberg, A. F. and G. L. Mellor. 1983. Diagnostic and prognostic numerical circulation studies in the South Atlantic Bight. Journal of Geophysical Research, 88:

Beardsley, R. C., and W. C. Boicourt, On estuarine and continental-shelf circulation in the Middle Atlantic Bight, in Evolution of Physical Oceanography, edited by B. A. Warren and C. Wunsch, pg. 198- 234, MIT Press, Cambridge, Mass., 1981.

Blumberg, A. F., Numerical tidal model of Chesapeake bay, J. Hydraul. Div., 103, 1-10, 1977.

Blumberg, A. F., and G. L. Mellor, A whole basin model of the Gulf of Mexico. Proc. 6th Ann. Conf. on OTEC, Department of Energy, Washington, D.C., 13.15-1 to 13.15-10, 1979a.

Blumberg, A. F., and G. L. Mellor, The potential impact of three-dimensional circulation modelling on oil spill forecasting, in The Physical Behavior of Oil in the Marine Environment, Princeton University, Department of Civil Engineering, 6.1-6.18, 1979b.

Blumberg, A. F., and G. L. Mellor, A Coastal ocean numerical Model, in mathematical Modelling of Estuarine Physics, Proc. Int. Symp., Hamburg, August 24-6, 1978. edited by J. Sundermann and K. –P. Holz, 203 –214, Springer-Verlag, Berlin, 1980.

Blumberg, A. F., and G. L. Mellor, A numerical calculation of the circulation in the Gulf of Mexico, Dunalysis of Princeton, Report No. 66, 153 pp., 1981*a*.

Blumberg, A. F., and G. L. Mellor, Circulation studies in the South Atlantic Bight with prognostic and diagnostic numerical models, *Rep. 71,* Dynalysis of Princeton, Princeton, N. J., 1981*b*.

Blumberg, A. F., and L. H. Kantha, Open boundary condition for circulation models, J. Hydraul. Eng., 111, 237-255. 1985.

Bryan, K., A numerical method for the study of the circulation of the world ocean, J. Comput. Phys., 4, No. 3, 347-376, 1969.

Fofonoff, N. P., Physical properties of sea-water, in The Sea Vol. 1, edited by N. M. Hill, pp. 3-30, Interscience, New York, 1962.

Kantha, L. H., G. L. Mellor, and A. F. Blumberg, A diagnostic calculation of the general circulation in the south Atlntic Bight, J. Phys. Oceanogr., 12, 805-819, 1982.

Mellor, G. L., and T. Yamada, Development of a turbulence closure model for geophysical fluid problems, Rev. Geophys. Space Phys., 20, No. 4, 851-875, 1982.

Smagorinsky, J., General circulation experiments with the primitive equations, I. The bsic experiment, Mon. Weather Rev., 91, 99-164, 1963.

Weatherly, G., and P. J. Martin, On the structure and dynamics of the ocean bottom boundary layer, J. Phys. Oceanogr., 8, 557-570, 1978.

Watanabe, M., Amano, K, Ishikawa, Y. and Kohata, K. Analysis of autumu upwelling of anoxic bottom water, destratificaition and vertical circulation induced by wind in Tokyo Bay. 1998.

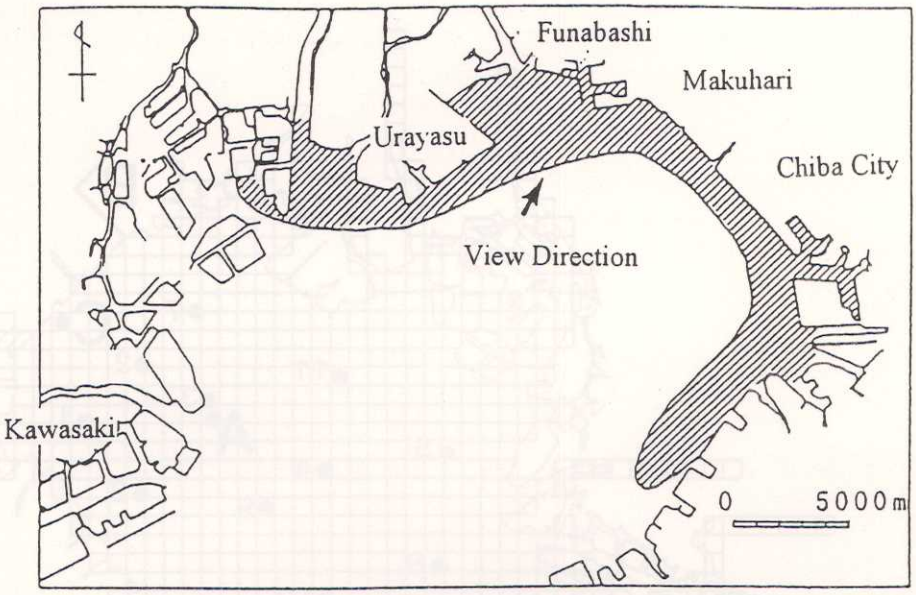

Figure 3.1 Area covered by Awoshiwo events (above) and an aerial picture of an Awoshiwo outbreak in Tokyo Bay (below, by courtesy of Asahi Shimbun).

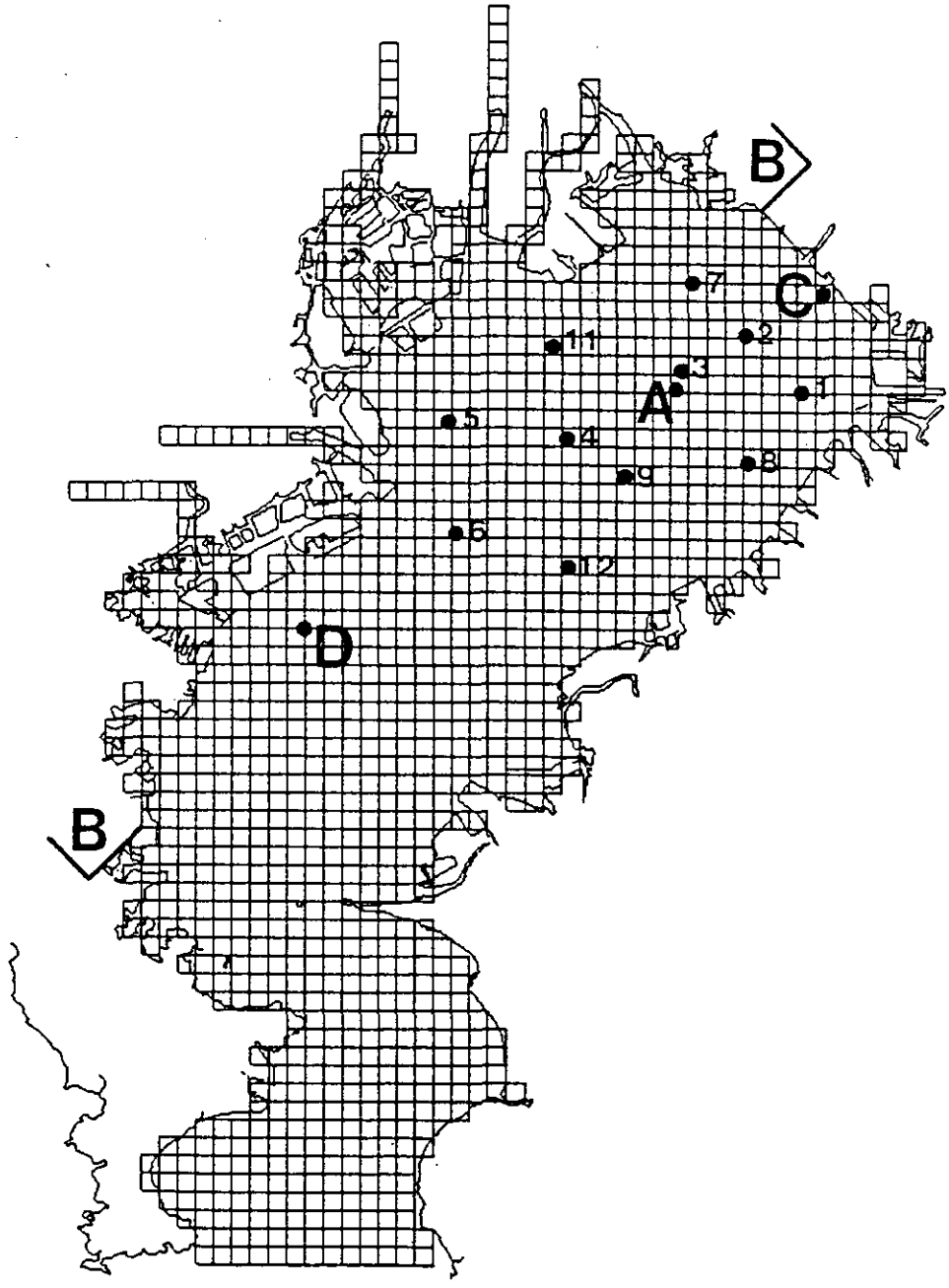

Figure 3.2 Plan view of the grid used for calculation, and locations of observations.

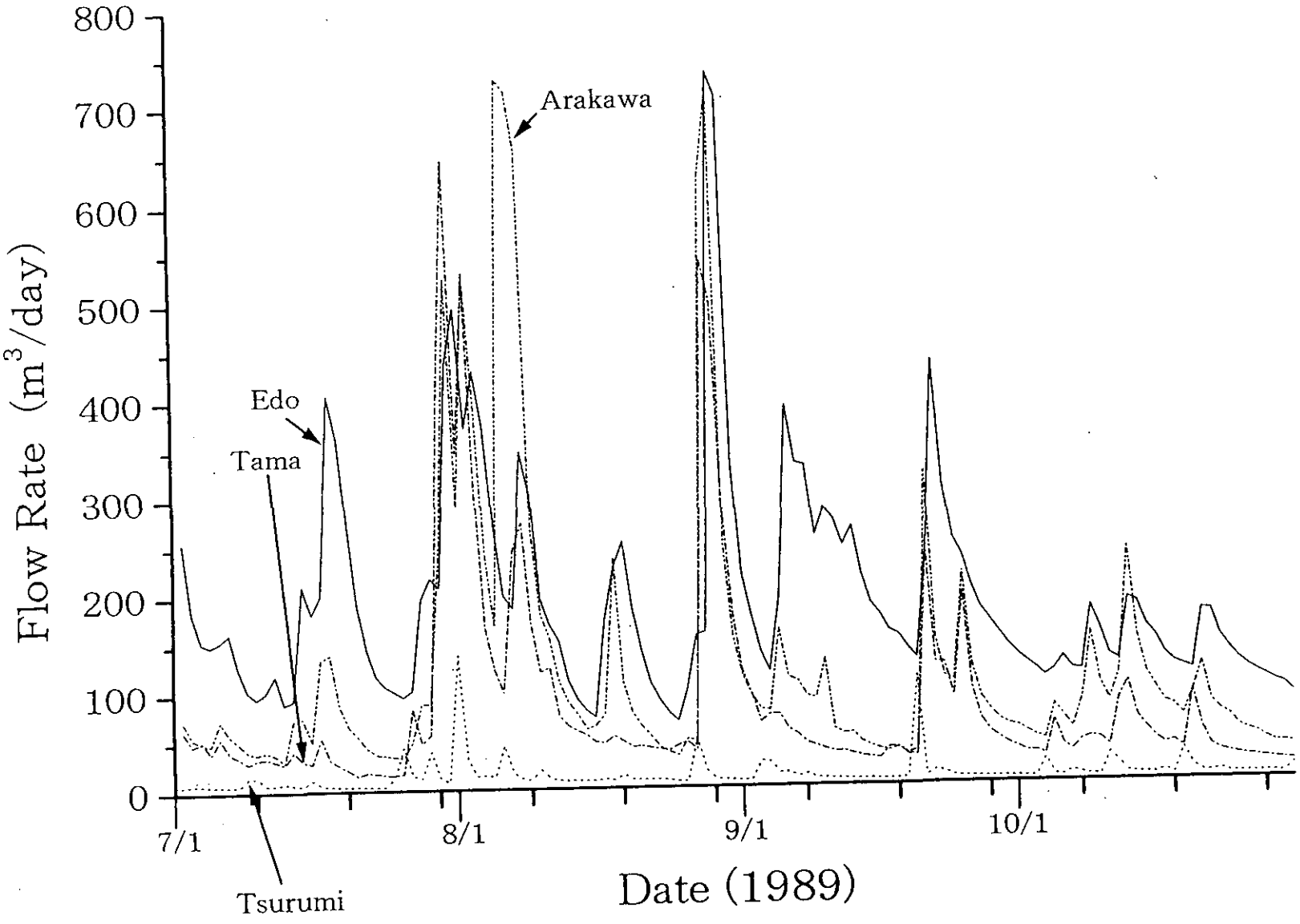

Figure 3.3 Flow rates of the Tsurumi, Tama, Ara and Edo rivers.

Figure 3.4 Freshwater discharge from POTW, factories and power stations along the shore of Tokyo Bay.

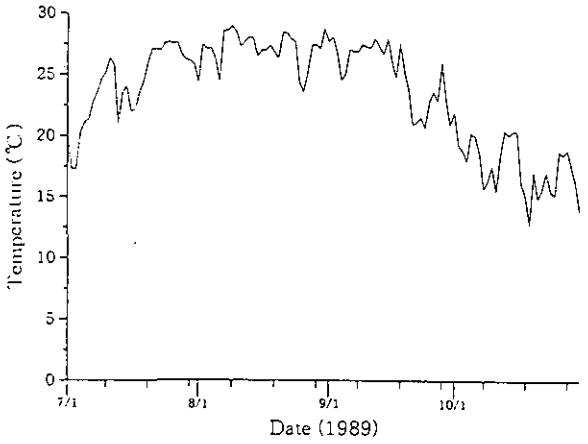

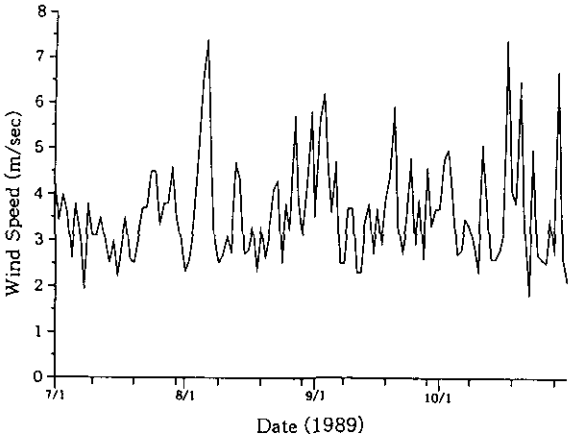

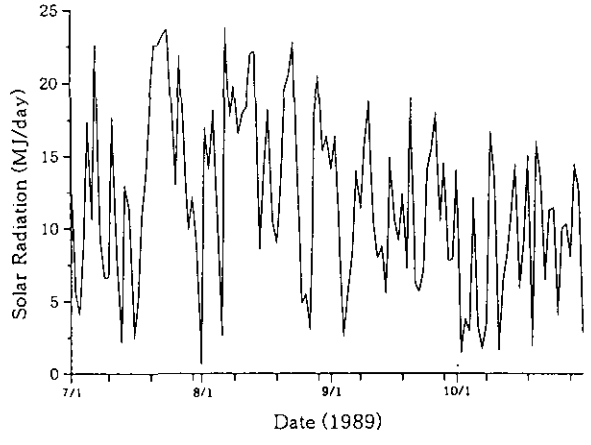

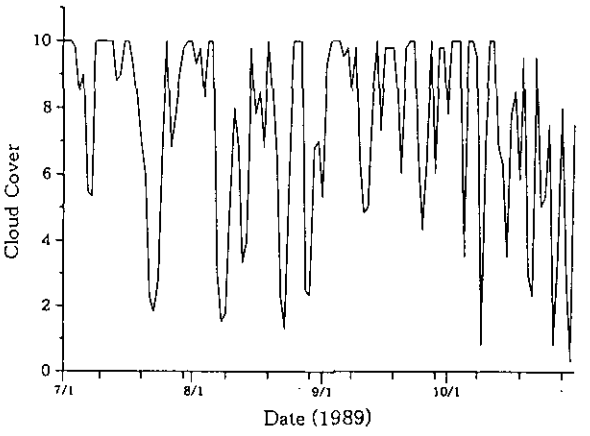

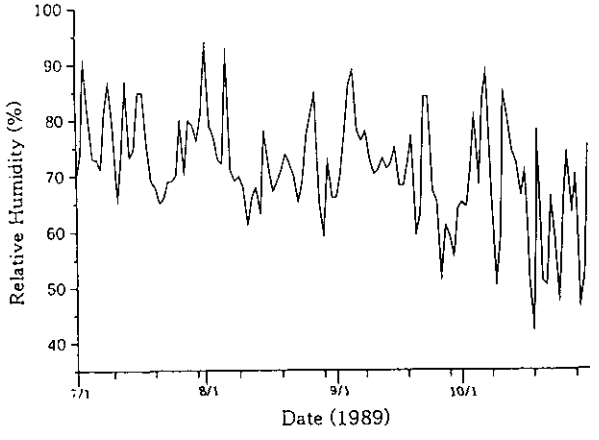

Figure 3.5 Temperature, solar radiation, relative humidity, wind speed and cloud cover observed by the Meteorological Agency at its observation station in Tokyo.

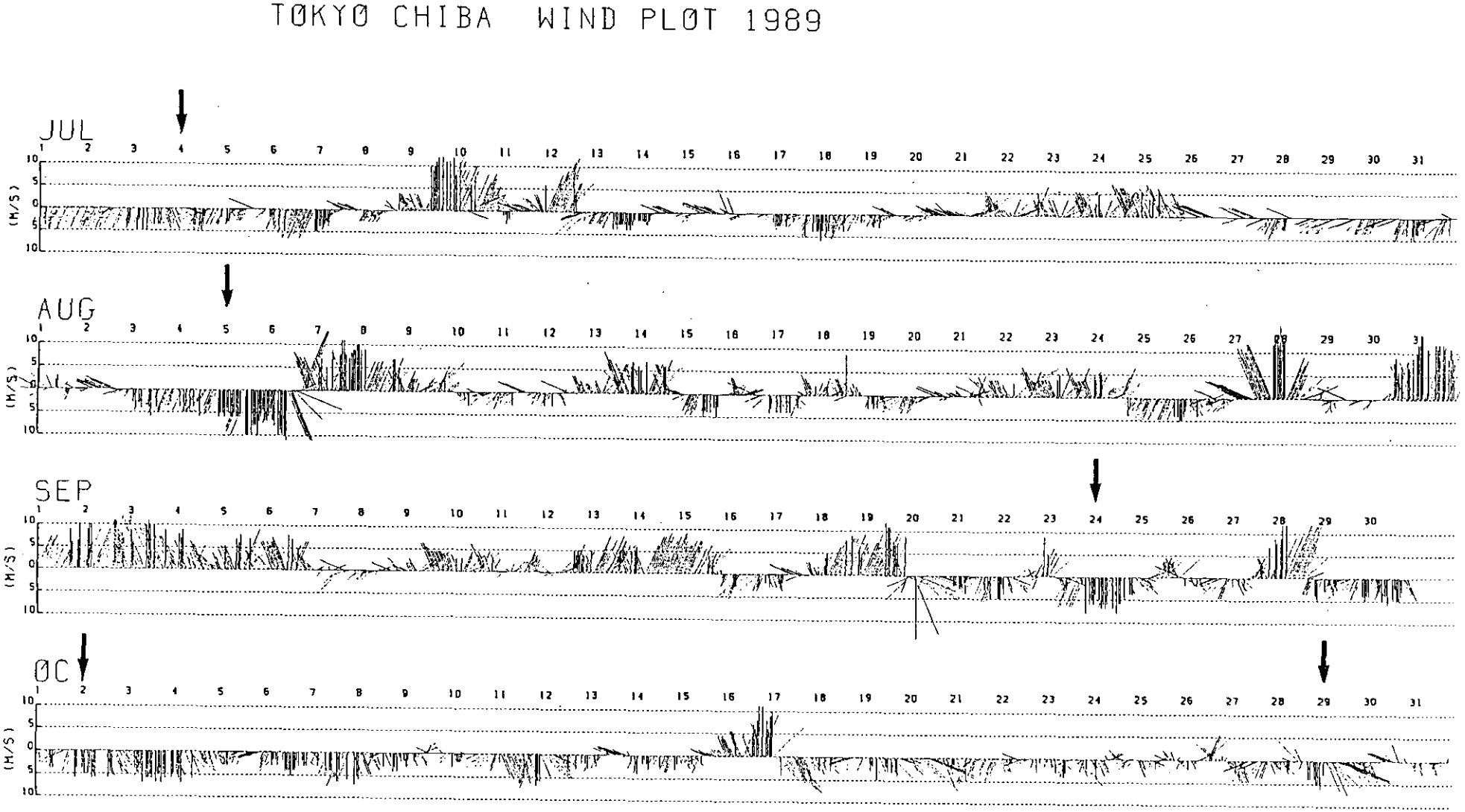

Figure 3.6 Observed wind speed and direction (Mean of Chiba, Kisarazu and Tokyo heliport stations).

(a)

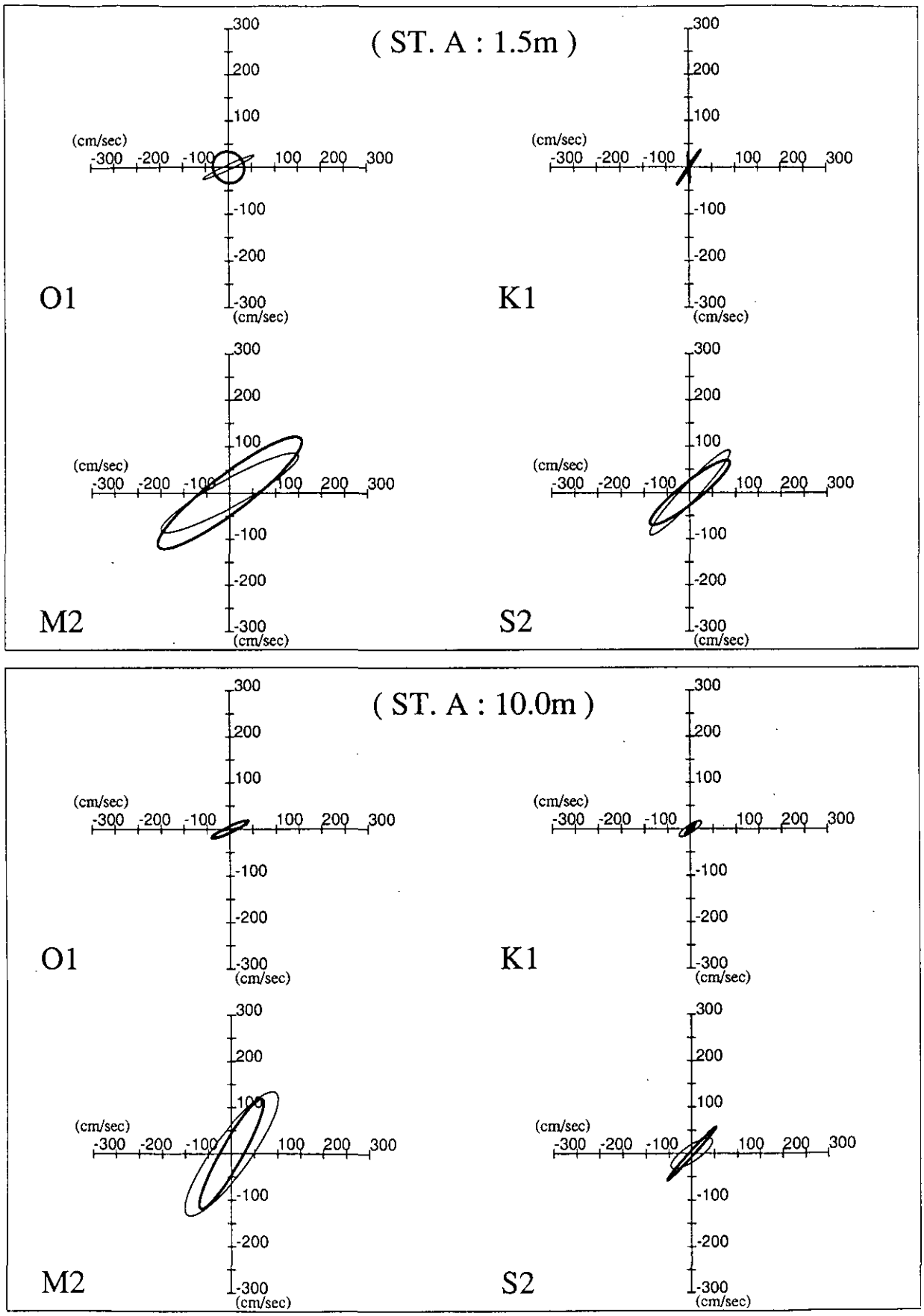

Figure 3.7 (a) Comparison of tidal ellipses for measured (——) and simulated (▬▬) currents at Station A.

(b)

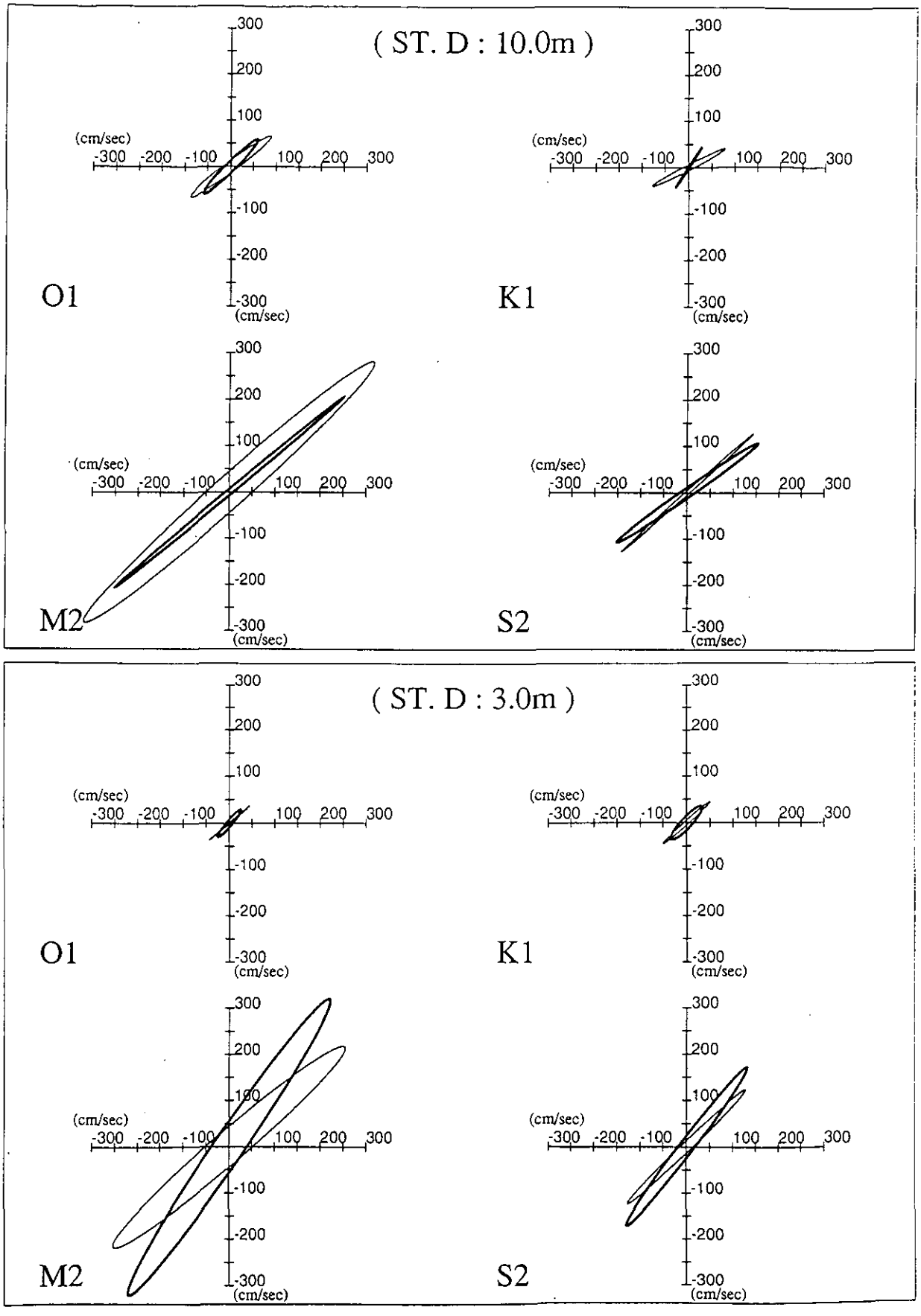

Figure 3.7 (b) Comparison of tidal ellipses for measured (——) and simulated (▬) currents at Station D.

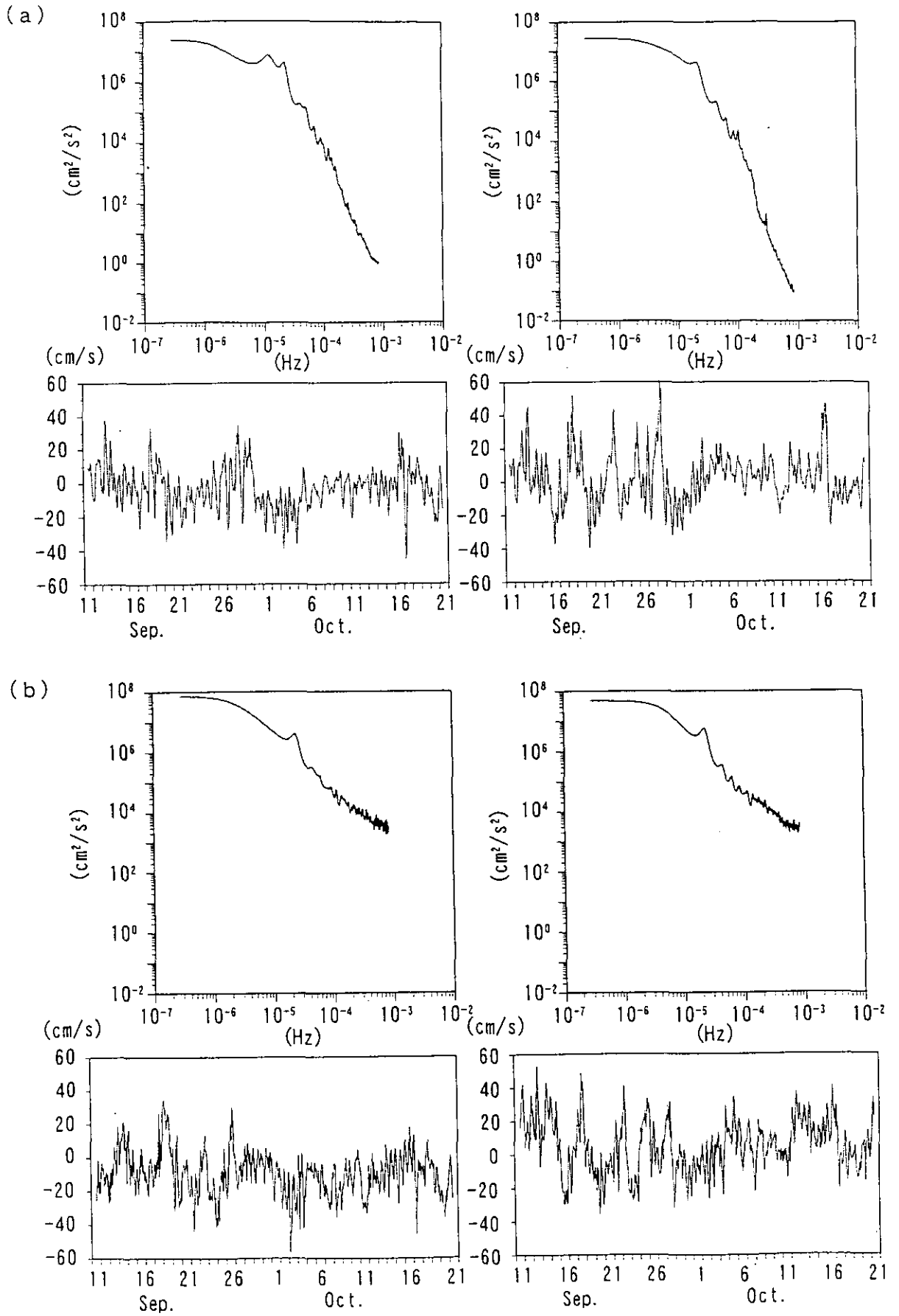

Figure 3.8 Velocity fluctuation and energy spectra for north-south (left) and east-west (right) directions at St. A. (a) calculated results; (b) observed results.

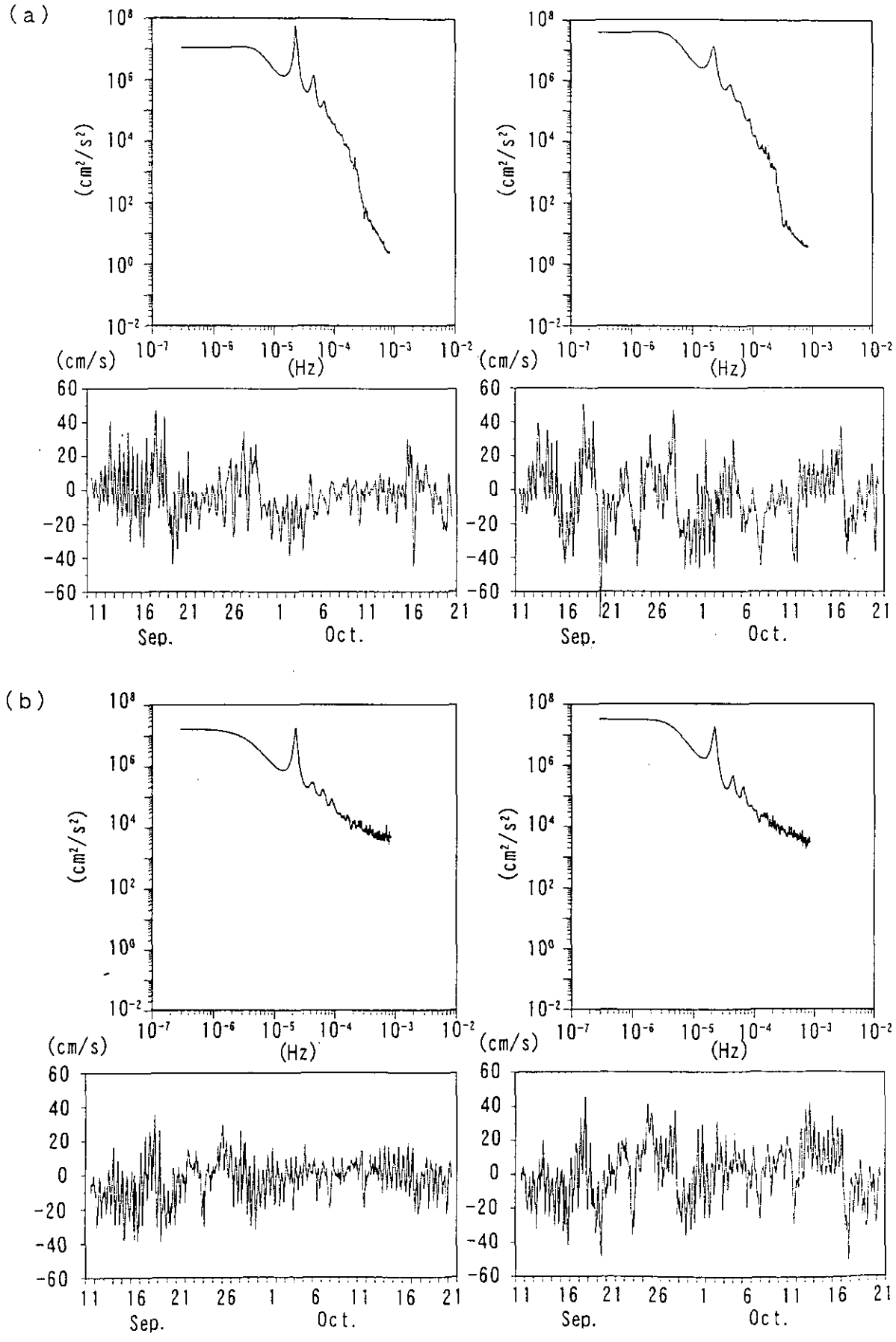

Figure 3.9 Velocity fluctuation and energy spectra for north-south (left) and east-west (right) directions at St. D. (a) calculated results; (b) observed results.

(a)

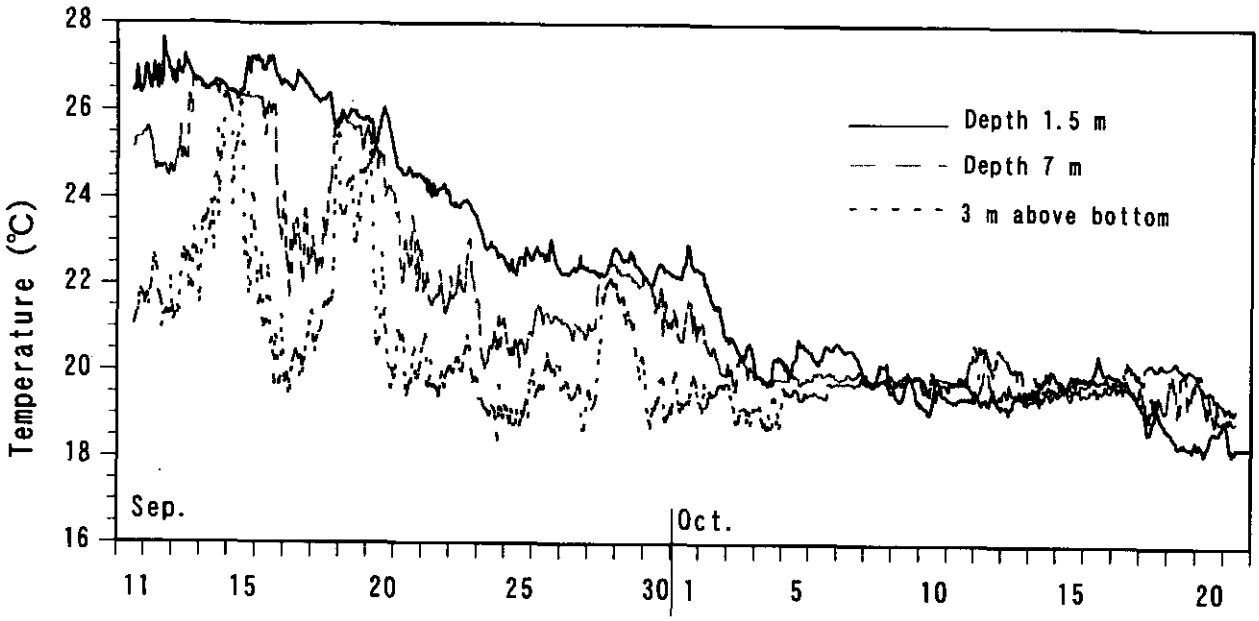

(b)

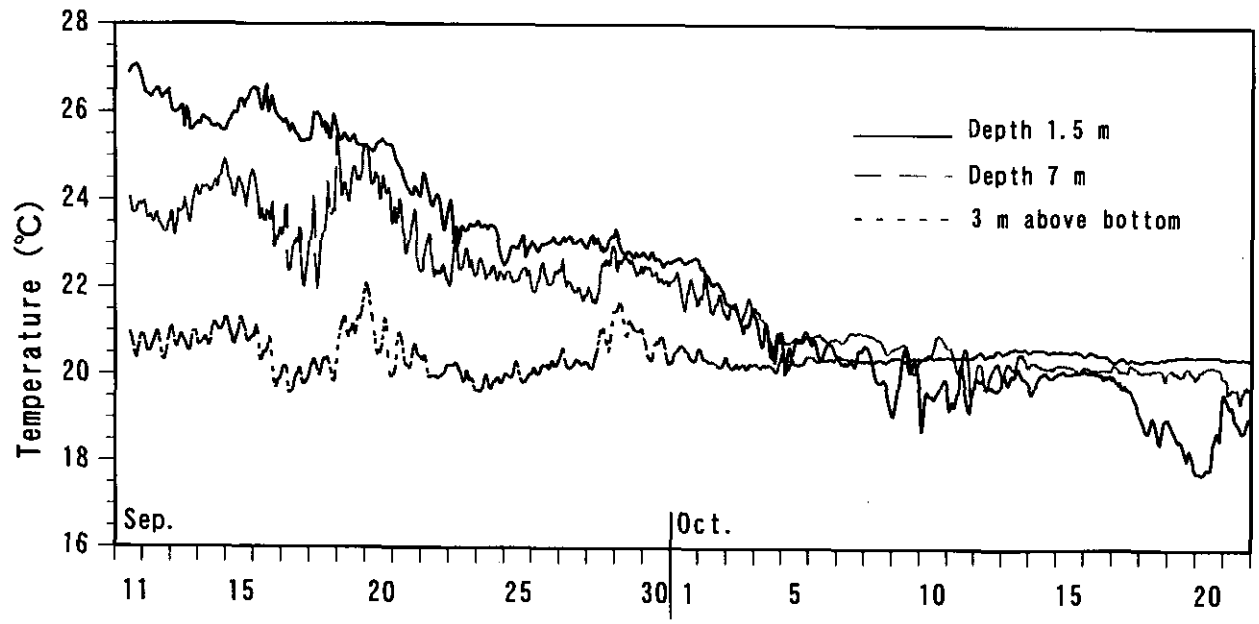

Figure 3.10 Temperature variation at St. A. (a) observed; (b) simulated.

(a)

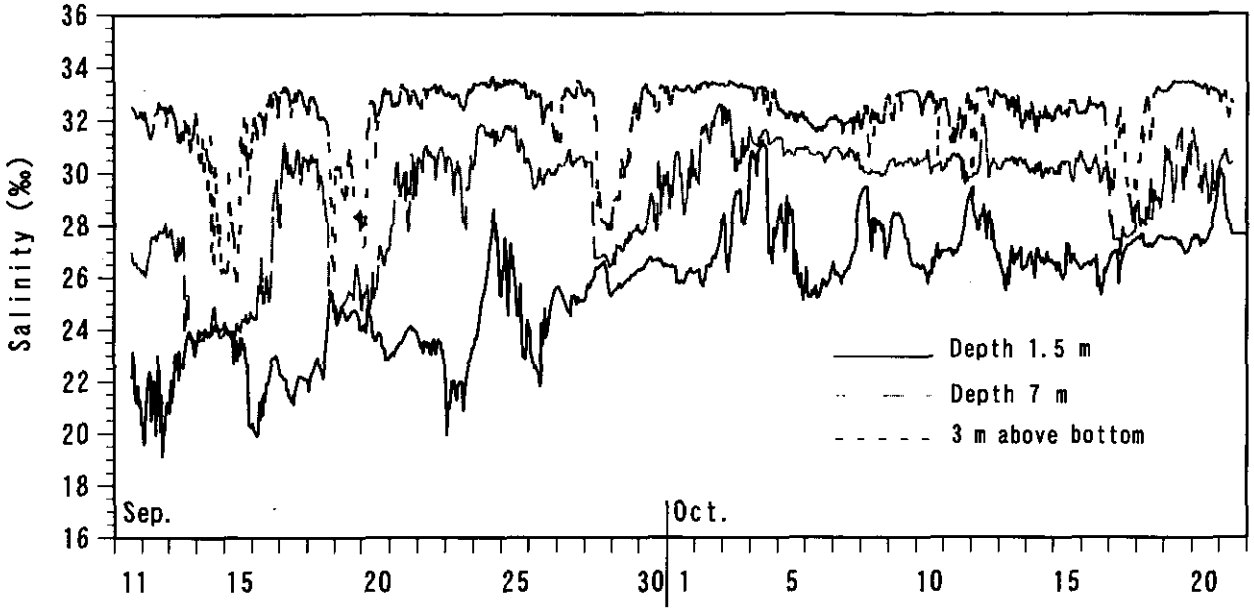

(b)

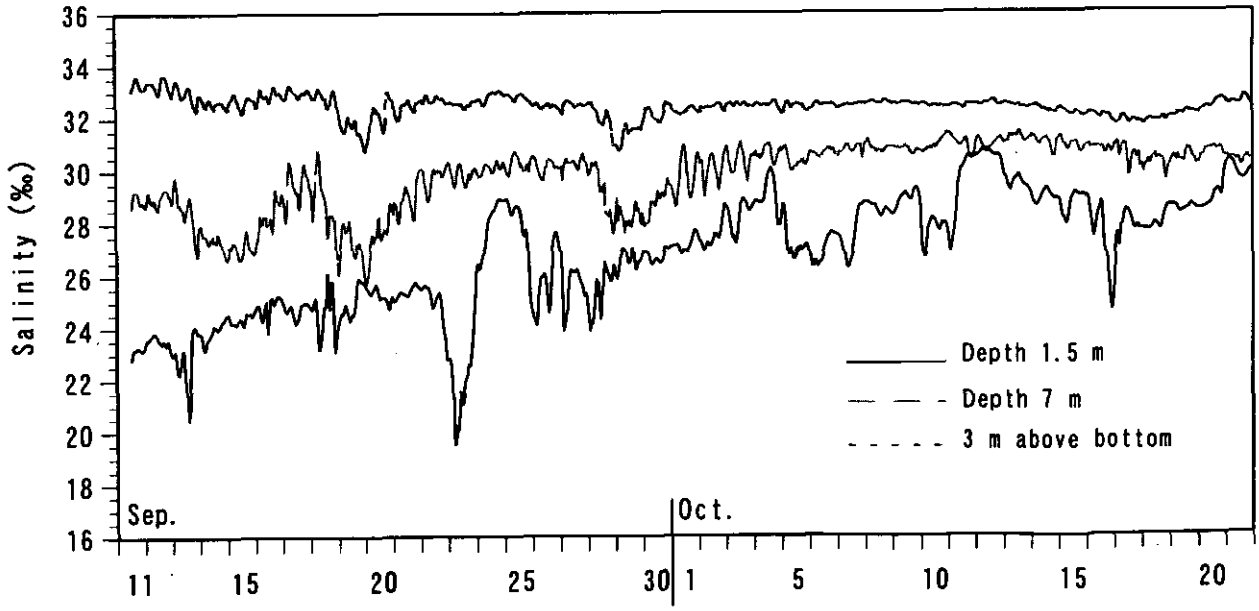

Figure 3.11 Salinity variation at St. A. (a) observed; (b) simulated.

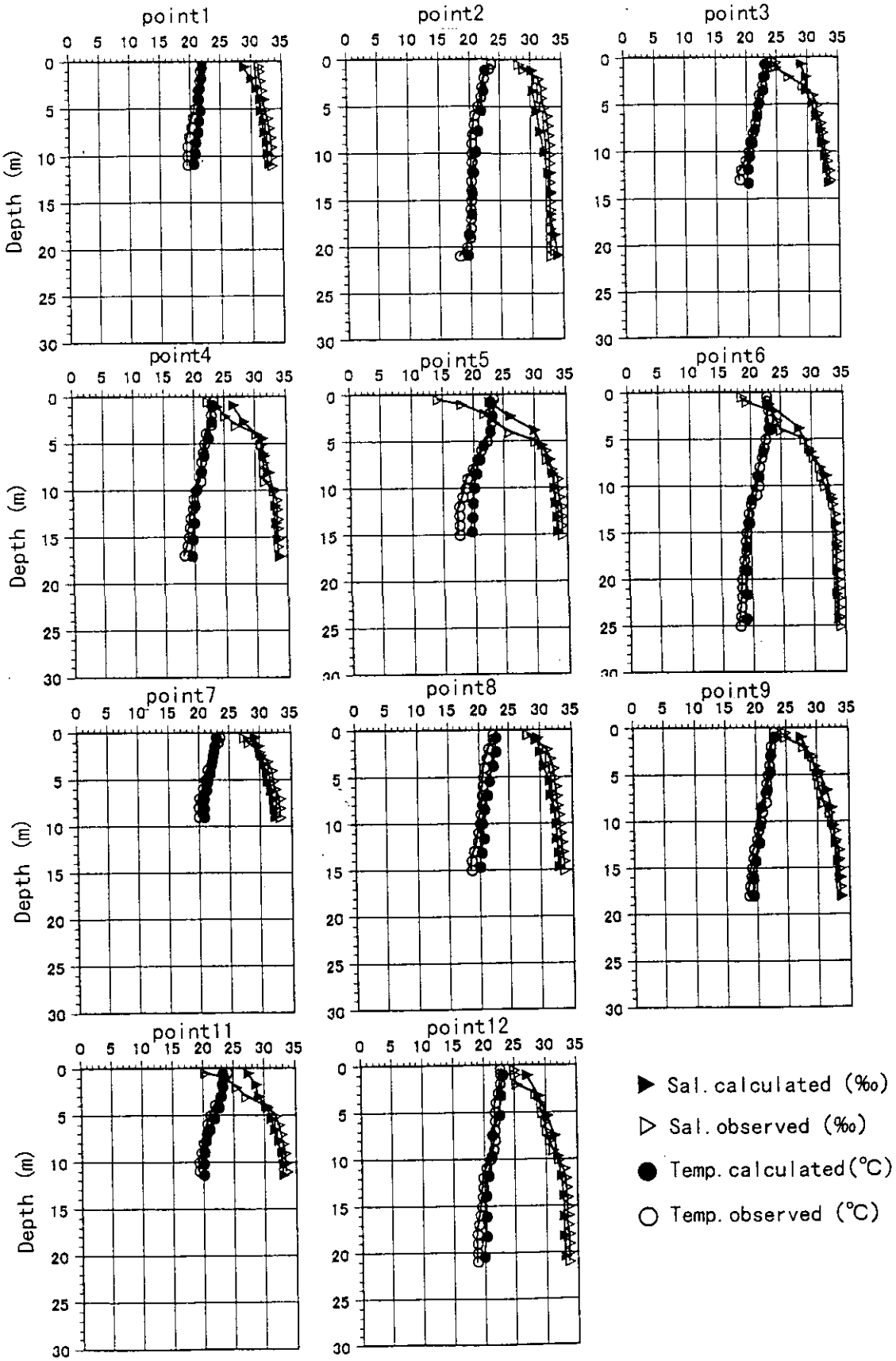

Figure 3.12 Vertical profiles of temperature and salinity at the observation points. (25 September 1989).

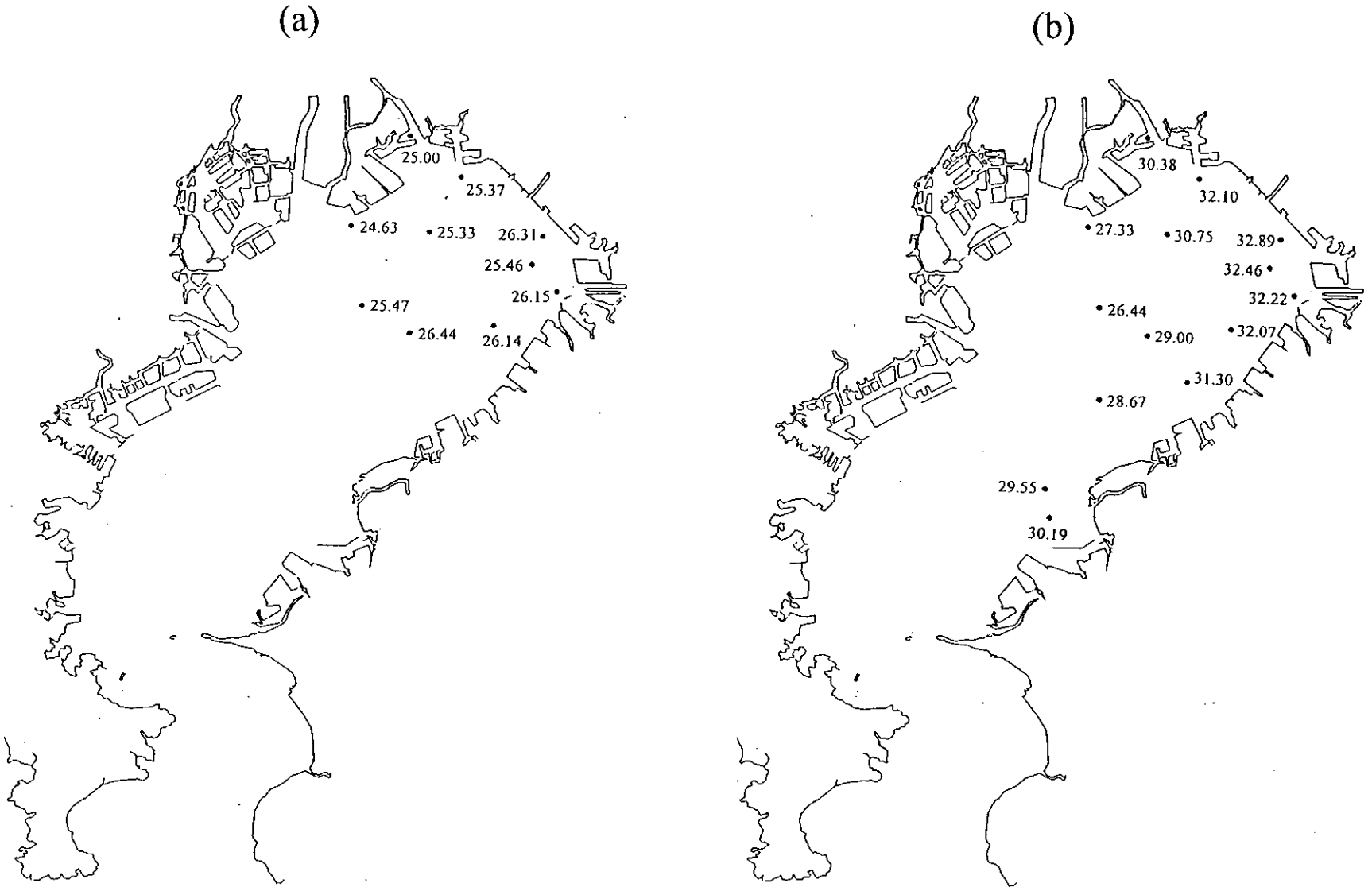

Figure 3. 13 Observed surface salinity (in ‰). (a) 27 September; (b) 3 October.

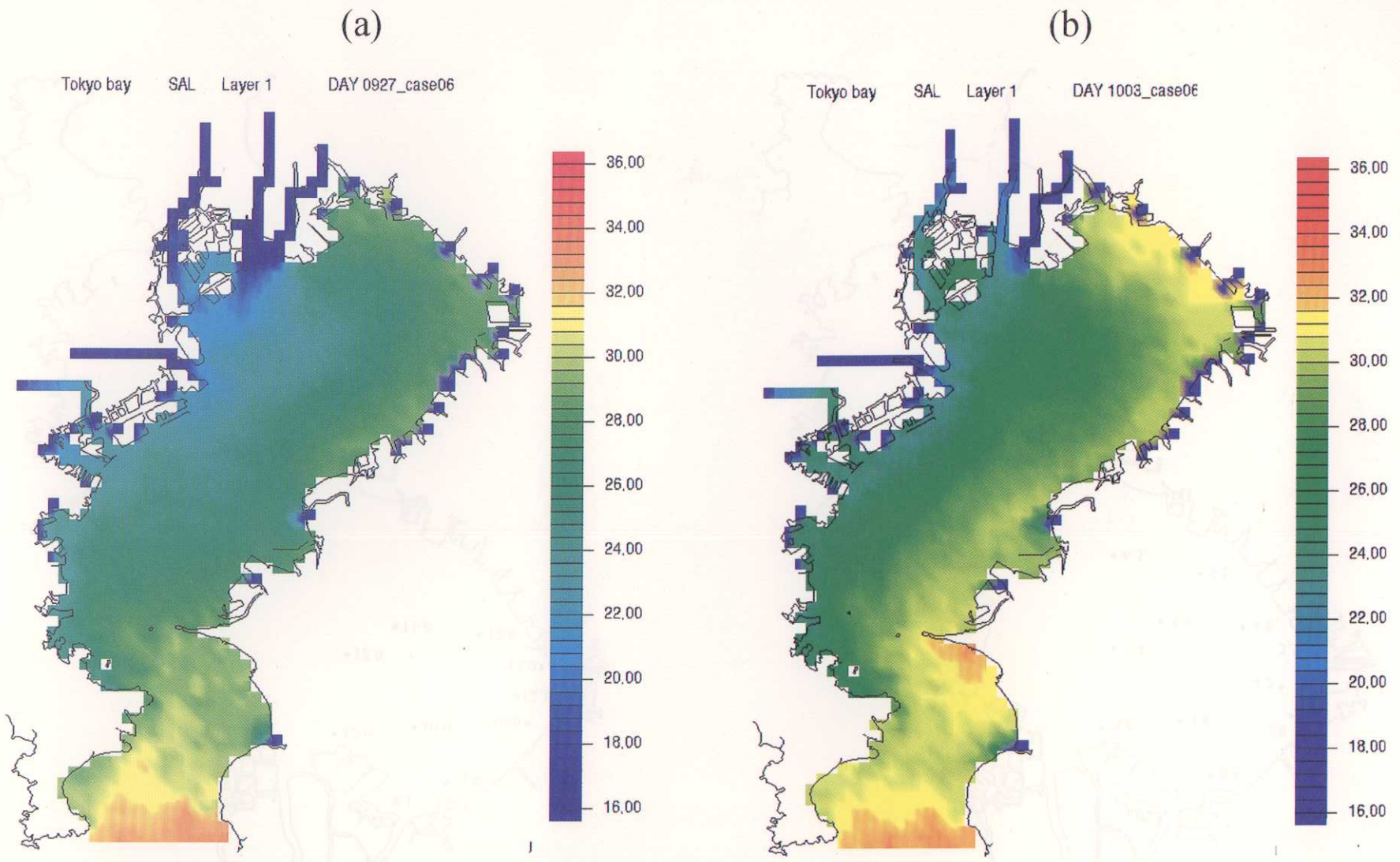

Figure 3. 14 Calculated surface salinity (in ‰). (a) 27 September; (b) 3 October.

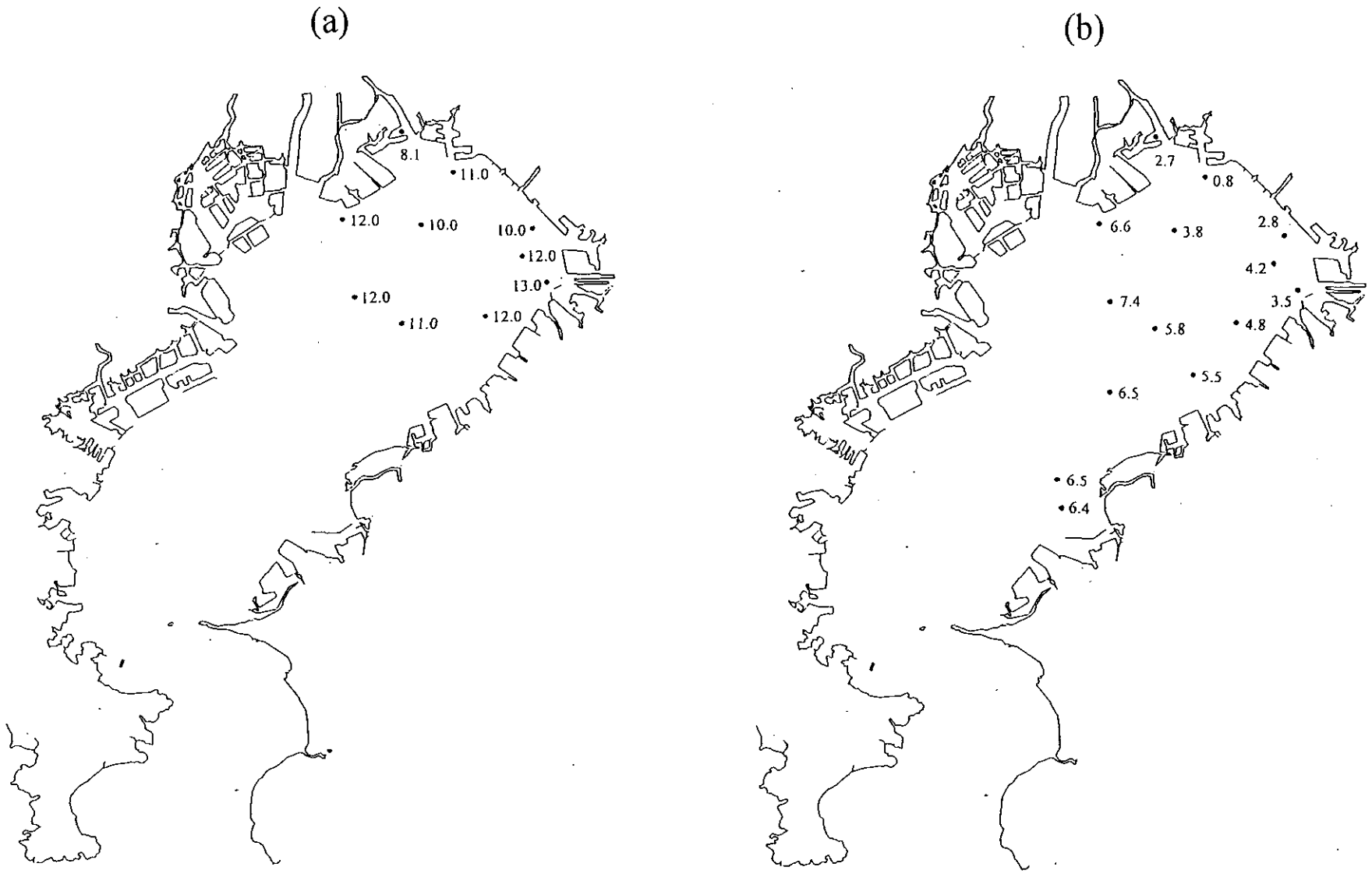

Figure 3. 15 Observed surface dissolved oxygen (in $mg.l^{-1}$). (a) 27 September; (b) 3 October.

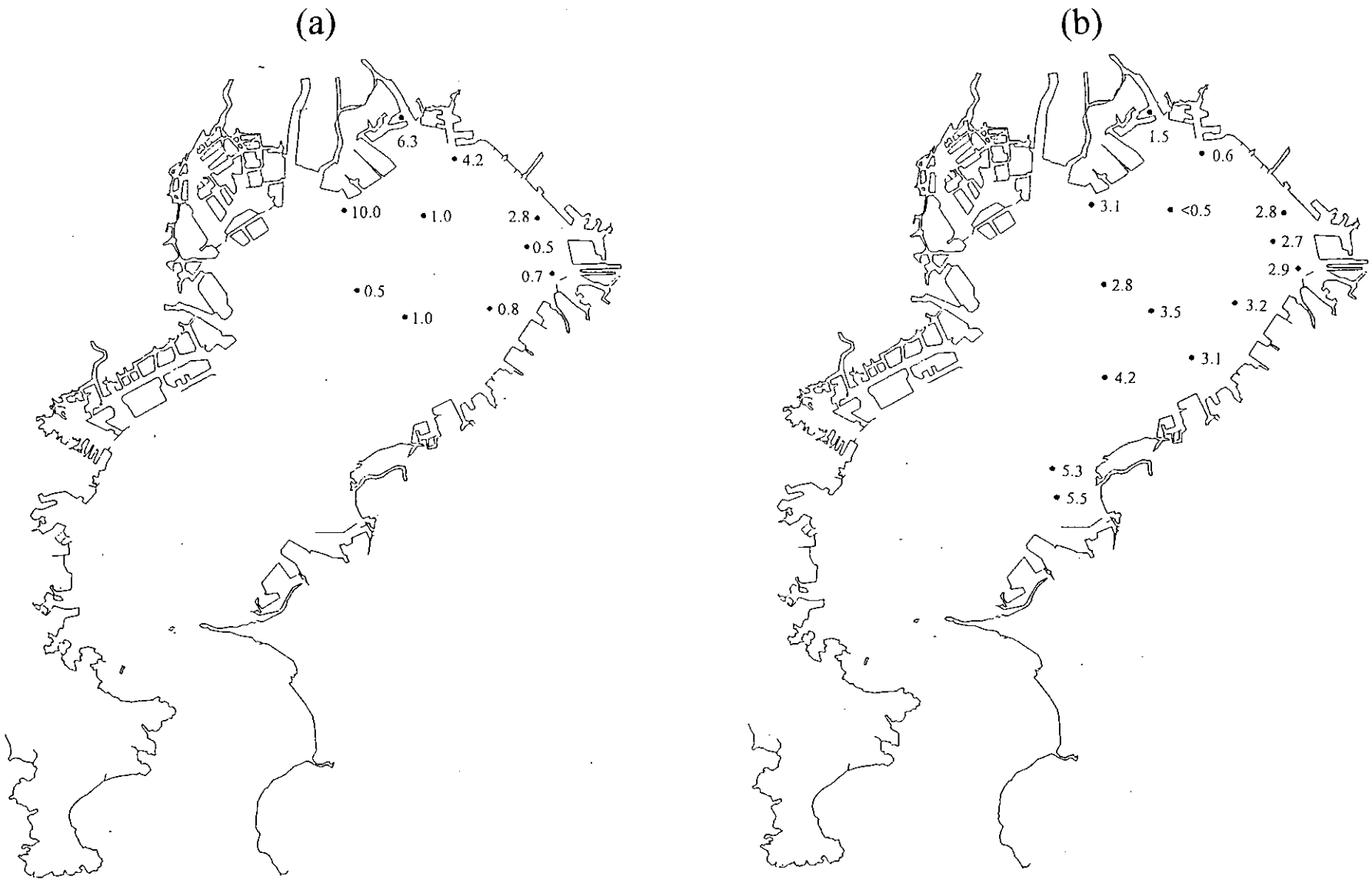

Figure 3. 16 Observed bottom dissolved oxygen in ($mg.l^{-1}$). (a) 27 September; (b) 3 October.

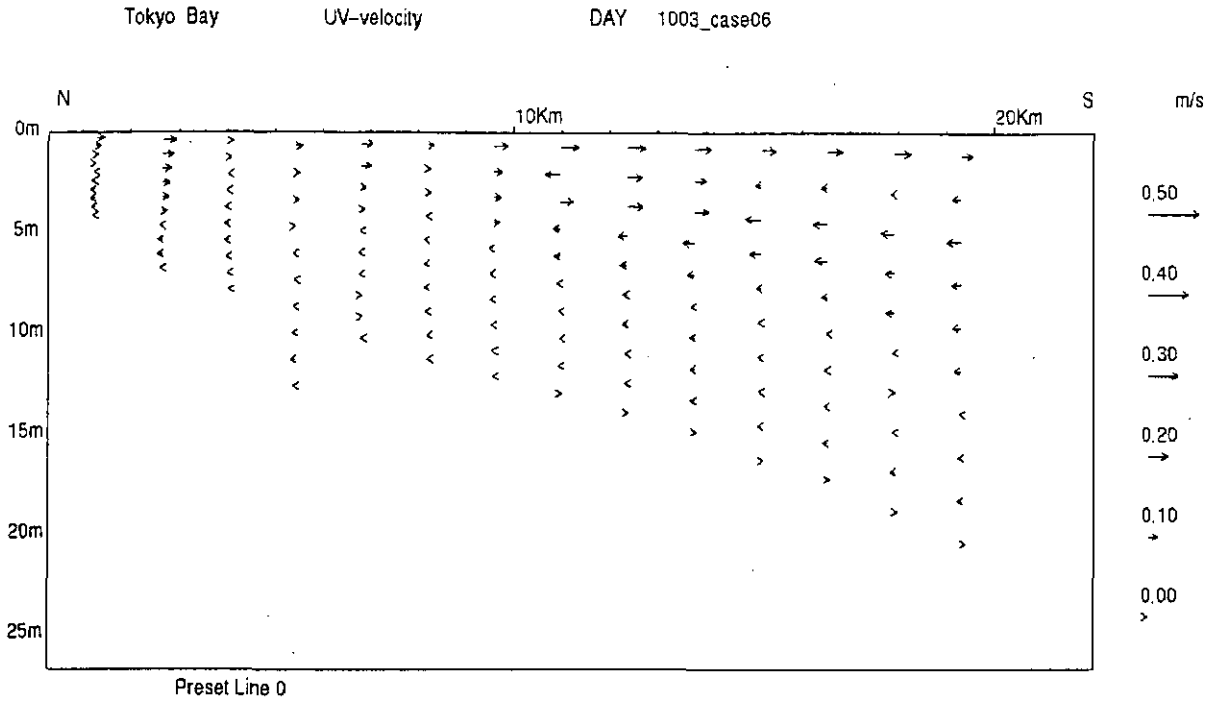

Figure 3.17 Horizontal velocity profile within the B-B cross-section shown in Fig. 3.2, 3 October.

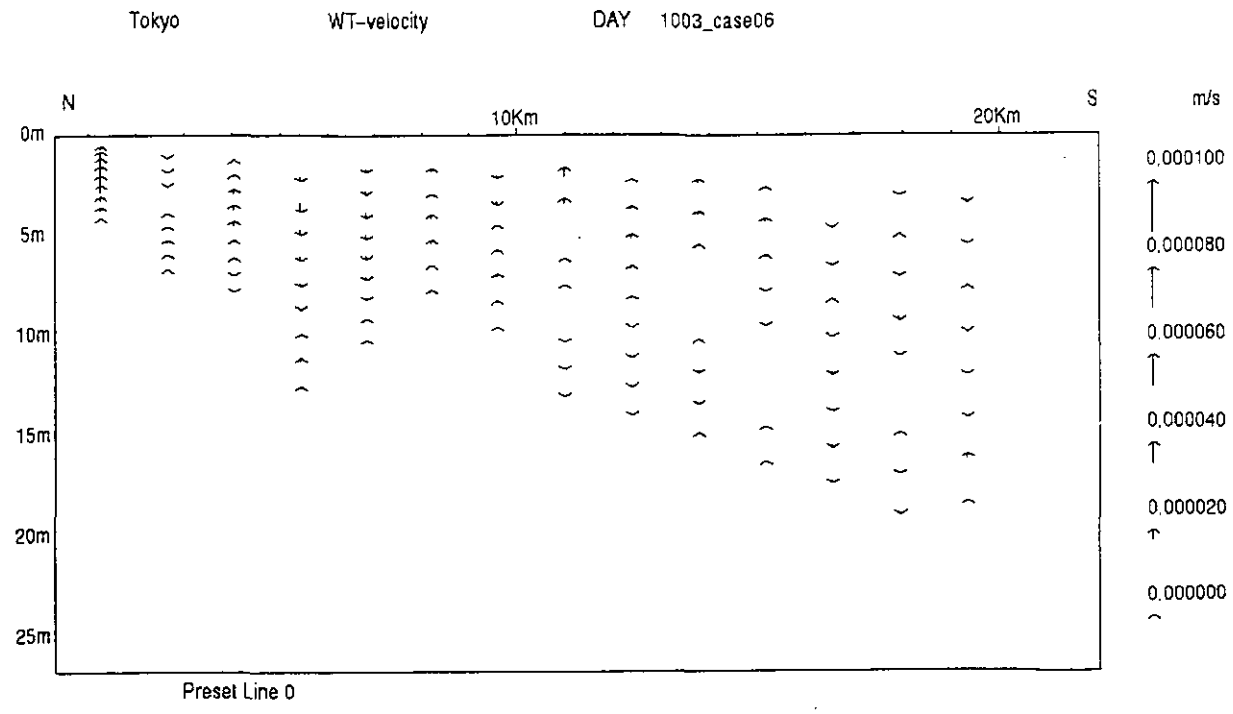

Figure 3.18 Vertical velocity profile within the B-B cross-section shown in Fig, 3,2, 3 October.

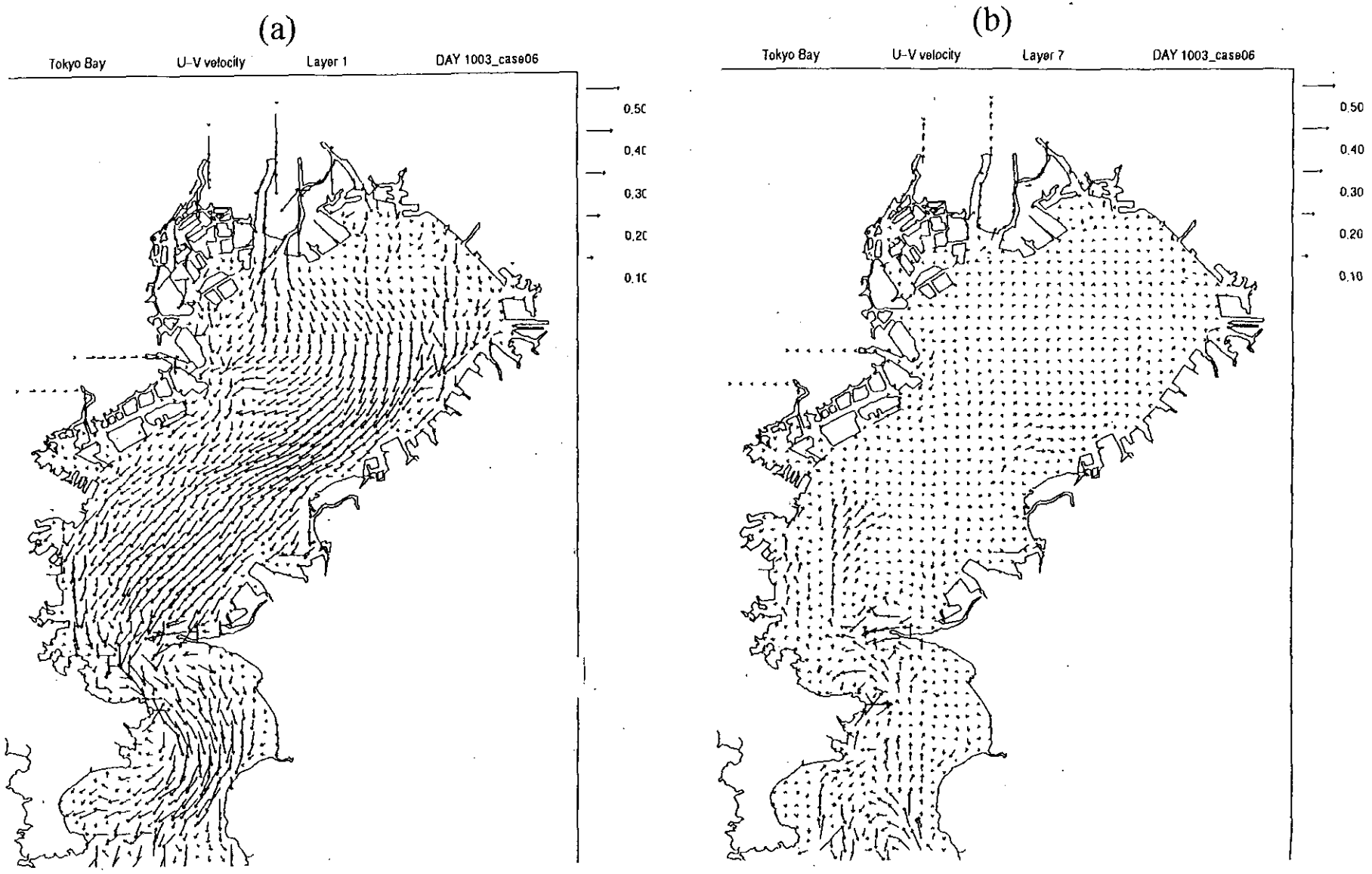

Figure 3. 19 Calculated horizontal velocity profiles on 3 October. (a) surface; (b) bottom.

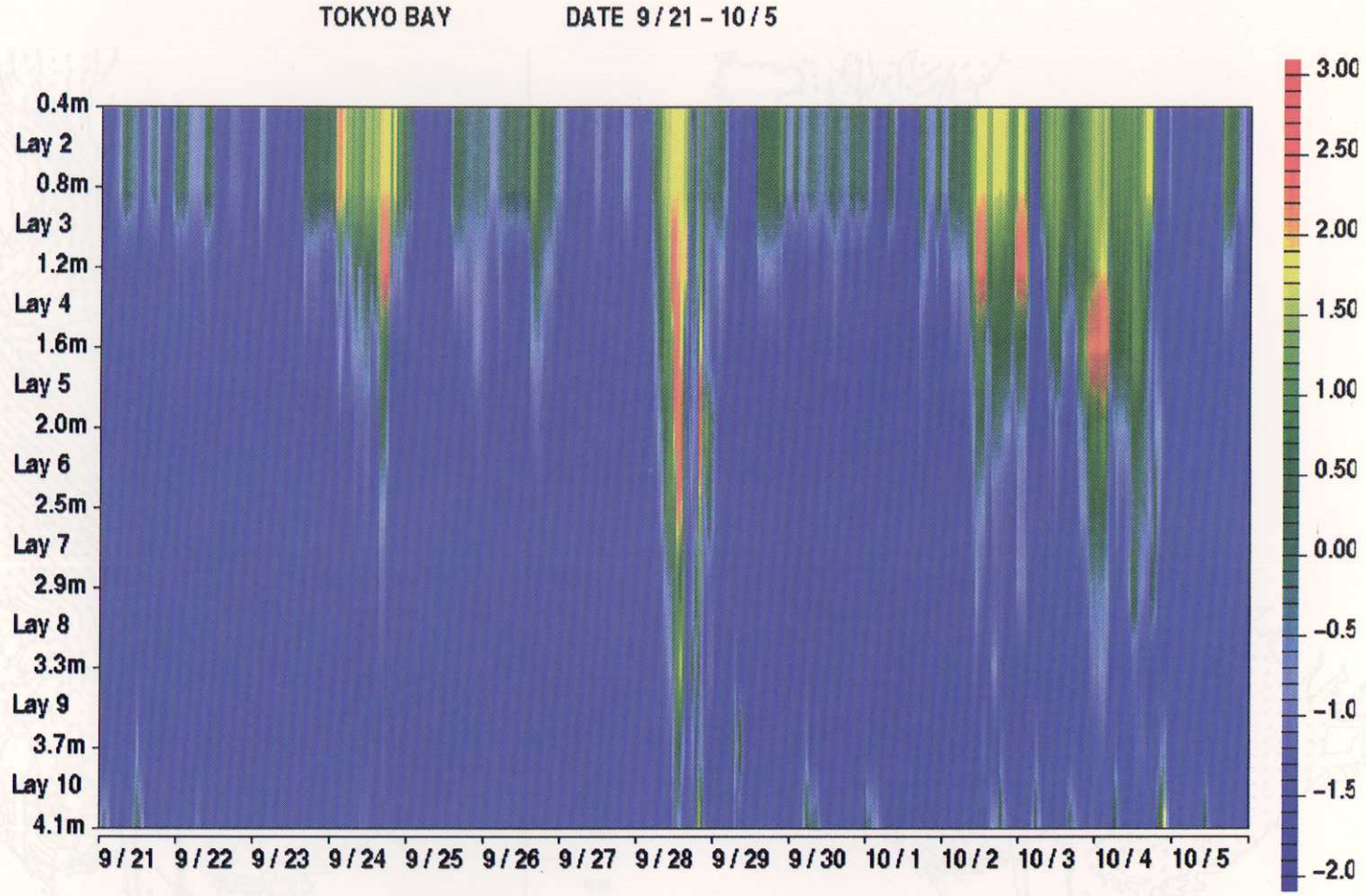

Figure 3.20 Vertical eddy-diffusivity change at St. C (in $\log(K_H)$).

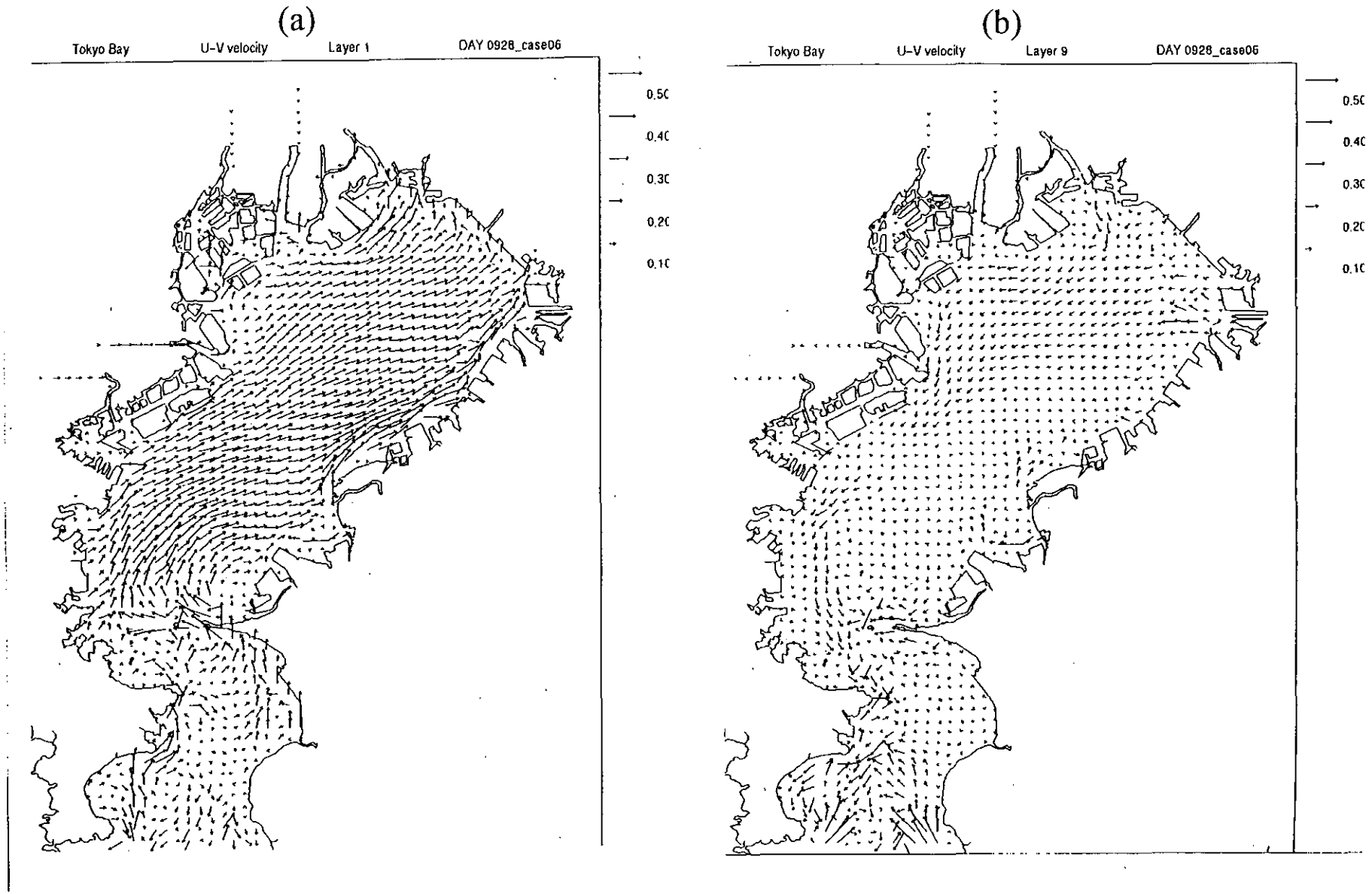

Figure 3. 21 Calculated horizontal velocity profiles on 28 September. (a) surface; (b) bottom.

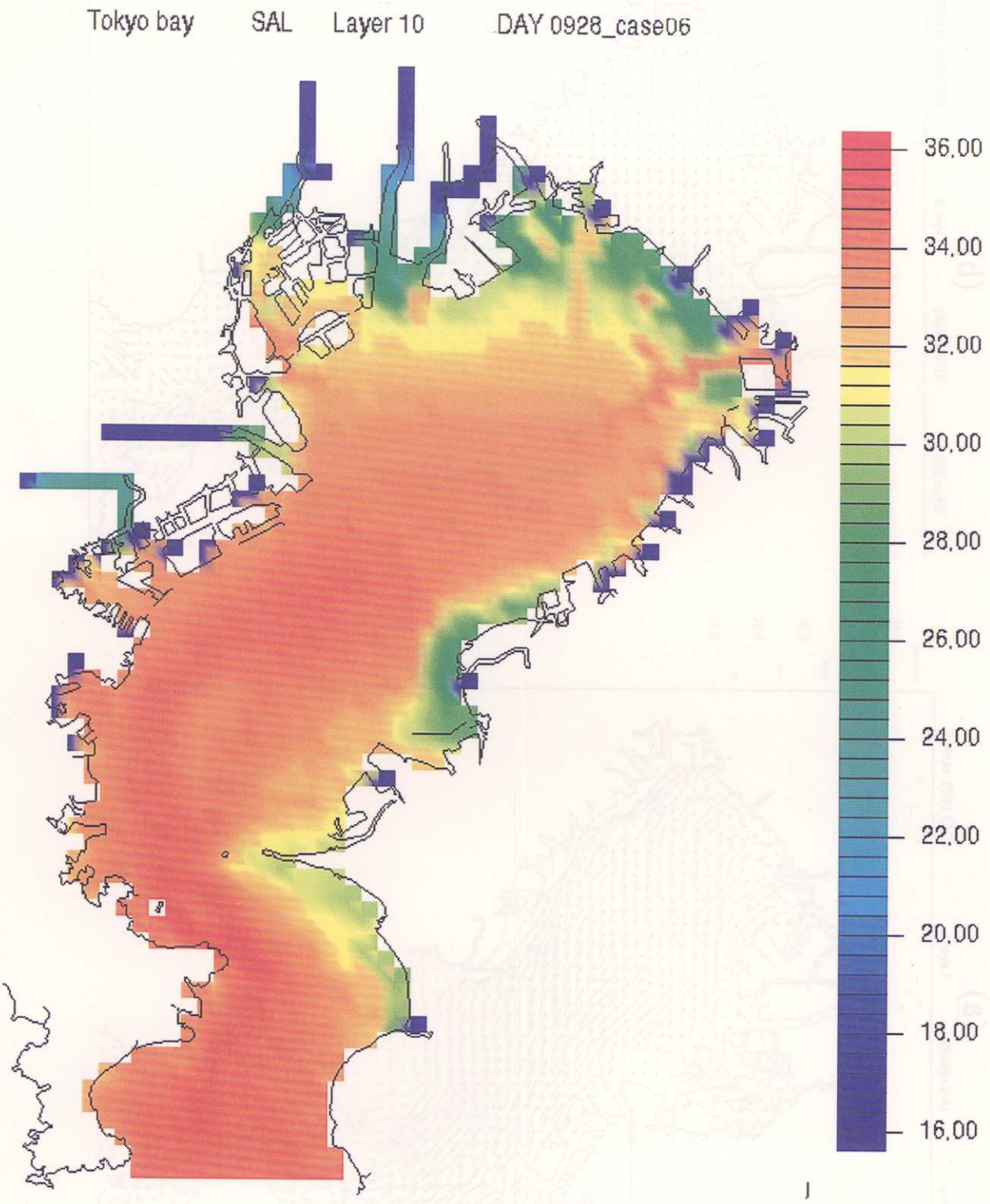

Figure 3. 22 Horizontal bottom salinity profile (in ‰), calculated for 28 September.

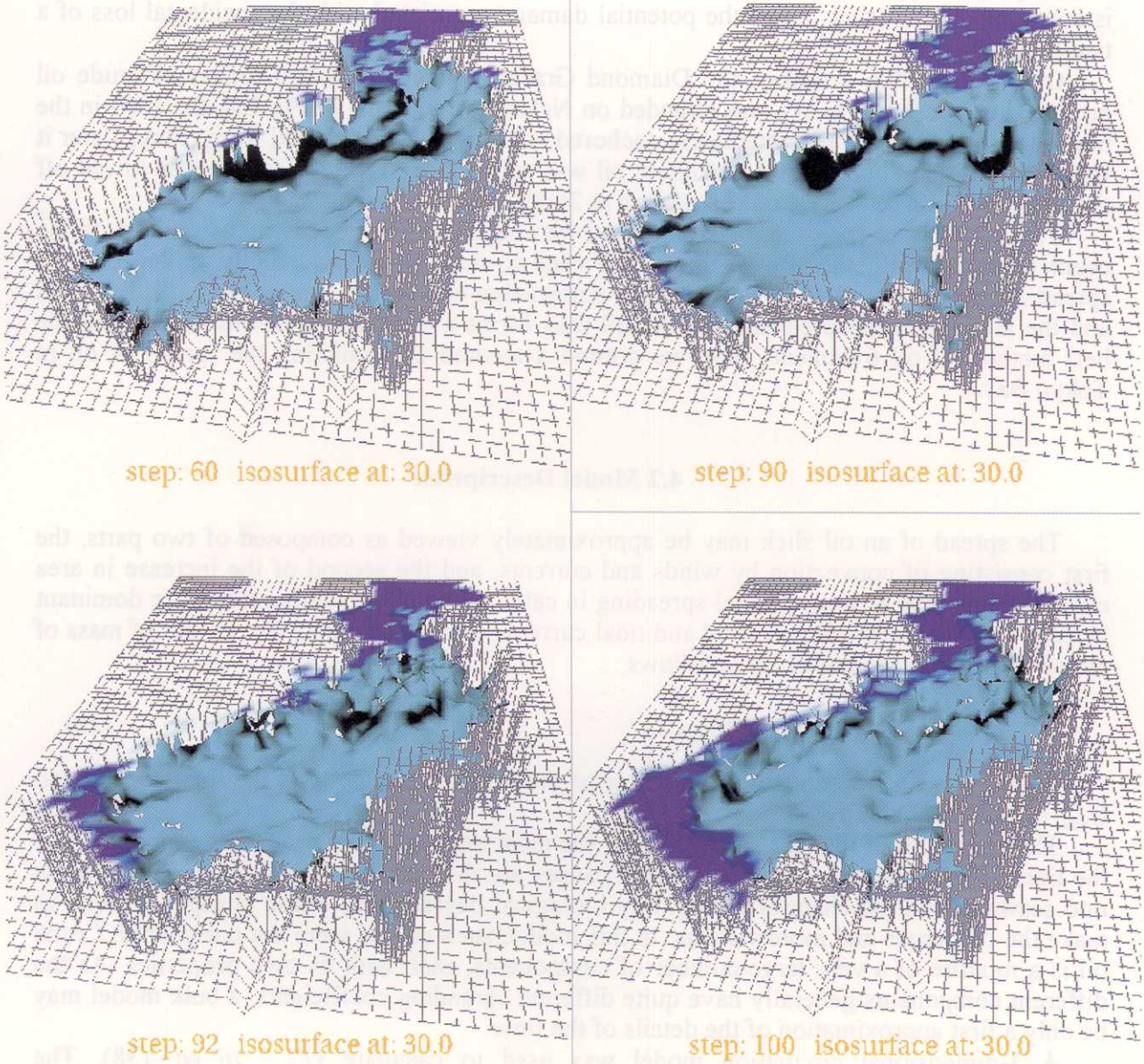

Figure 3.23 Three-dimensional views of contours of 30‰ isohalines, and surface area where salinity was higher than 30‰. (Oct. 2 and 3, 1989)